Josephson current through superconductor/diffusive-normal-metal/superconductor junctions: Interference effects governed by pairing symmetry

Yasuhiro Asano*
Department of Applied Physics, Hokkaido University, Sapporo 060-8628, Japan

Yukio Tanaka and Takehito Yokoyama
Department of Applied Physics, Nagoya University, Nagoya 464-8603, Japan
and CREST, Japan Science and Technology Corporation (JST) Nagoya, 464-8603, Japan

Satoshi Kashiwaya
National Institute of Advanced Industrial Science and Technology, Tsukuba 305-8568, Japan
(Received 17 April 2006; published 17 August 2006)

The Josephson effect in superconductor/diffusive-normal-metal/superconductor junctions is studied numerically by using the recursive Green function method. In superconductors, we consider spin-singlet *s*- and *d*-wave and spin-triplet *p*-wave pairing symmetries. The pairing symmetry governs two interference effects in junctions: the formation of a midgap Andreev resonant state at junction interfaces and the proximity effect in diffusive normal metals. A cooperative effect between the two interference effects causes anomalous Josephson current in a *p*-wave symmetry.

DOI: 10.1103/PhysRevB.74.064507 PACS number(s): 74.50.+r, 74.25.Fy, 74.70.Tx

I. INTRODUCTION

The Josephson effect is the highlight of superconducting phenomena.[1] The gradient in the macroscopic phase of superconductivity drives electric currents in equilibrium. A considerable number of theoretical studies have revealed the nature of the Josephson effect[2] since a Josephson current formula in superconductor/insulator/superconductor (SIS) junctions was derived based on a microscopic theory.[3] The Josephson current is also observed in superconductor/diffusive-normal-metal/superconductor (SNS) junctions, where the length of a normal metal is much larger than the mean free path due to elastic impurity scatterings.[2,4] In SNS junctions, the Josephson effect is understood in terms of the proximity effect; Cooper pairs penetrate into diffusive normal metals. In this sense, supercurrents flow as far as the amplitudes of the Cooper pairs are finite in diffusive normal metals. The applicability of these theories, however, is limited to superconducting junctions of conventional *s*-wave pairing symmetry.

In recent years, transport phenomena in unconventional superconductors have attracted considerable interest because high-T_c superconductivity is characterized by *d*-wave pairing symmetry.[5–7] Contrary to *s*-wave symmetry, the pair potentials in unconventional superconductors change their sign on the Fermi surface. It is now known that the sign change of pair potentials causes the formation of a midgap Andreev resonant state (MARS) at the surface of superconductors[8–12] because of the interference effect of a quasiparticle.[13] The MARS spatially localizes at a distance of $\xi_0=\hbar v_F/\pi\Delta_0$ from the surface[14] and energetically forms just on the Fermi energy, where ξ_0 is the coherence length, $v_F=\hbar k_F/m$ is the Fermi velocity, k_F is the Fermi wave number, and m is the mass of an electron. The low-temperature anomaly of the Josephson current in SIS junctions of unconventional superconductors[15–25] is a consequence of the resonant tunneling of Cooper pairs through the MARS.

The sign change of pair potentials affects also the proximity effect in diffusive normal metals. Suppression of the proximity effect is usually expected because the wave function of a Cooper pair originating from the positive part of pair potentials cancels that originating from the negative part. In fact, one of authors has shown that the ensemble average of the Josephson current vanishes in diffusive SNS junctions for several unconventional superconductors.[26,27] This phenomenon is now interpreted as the absence of the proximity effect in diffusive normal metals.[28,29] On the other hand, two of us discussed anomalous enhancement of the zero-bias tunneling conductance due to the proximity effect in the presence of the MARS.[30,31]

In this paper, we study the ensemble average of the Josephson current in SNS junctions of unconventional superconductors. The Josephson current in a single sample is calculated numerically by using the recursive Green function method.[32–34] After calculating the Josephson current for a number of SNS junctions with different impurity configurations, the ensemble average and the fluctuations are obtained. We consider spin-singlet *s*- and *d*-wave and spin-triplet *p*-wave pairing symmetries in superconductors. The Josephson effect depends strongly on the pairing symmetries because the two interference effects (the formation of the MARS and the proximity effect) are sensitive to pairing symmetries. We show that a cooperative effect between the midgap Andreev resonant states and the proximity effect causes anomalous Josephson current in a *p*-wave symmetry. A part of this paper has been already published elsewhere.[35]

This paper is organized as follows. In Sec. II, we discuss a relation between the pairing symmetry of superconductivity and the two interference effects of quasiparticles: the proximity effect and the MARS. The theoretical model and the method of simulation are explained in Sec. III. Numerical results of the Josephson current are discussed for four pairing symmetries in Sec. IV. The origin of the anomalous Joseph-

son effect in the p_x-wave symmetry is explained in Sec. IV. In Sec. VI, we summarize the paper. Throughout this paper, we take units of $\hbar = k_B = 1$, where k_B is the Boltzmann constant.

II. PAIRING SYMMETRIES

We consider five pairing symmetries in two-dimensional superconductors as follows:

$$\Delta_{\boldsymbol{k}}^{(s)} = \Delta_0, \tag{1}$$

$$\Delta_{\boldsymbol{k}}^{(d_{x^2-y^2})} = \Delta_0(\bar{k}_x^2 - \bar{k}_y^2), \tag{2}$$

$$\Delta_{\boldsymbol{k}}^{(d_{xy})} = \Delta_0 2\bar{k}_x\bar{k}_y, \tag{3}$$

$$\Delta_{\boldsymbol{k}}^{(p_y)} = \Delta_0\bar{k}_y, \tag{4}$$

$$\Delta_{\boldsymbol{k}}^{(p_x)} = \Delta_0\bar{k}_x, \tag{5}$$

where $\bar{k}_x = k_x/k_F$ and $\bar{k}_y = k_y/k_F$ are the normalized wave numbers on the Fermi surface in the x and y directions, respectively. In this section, we assume an isotropic Fermi surface in two-dimensional electron systems. Thus the relation $\bar{k}_x^2 + \bar{k}_y^2 = 1$ holds. The electric current is parallel to the x direction and the junction interface is parallel to the y direction as shown in Fig. 1(a). In Eqs. (1)–(5), we only consider the orbital part of the pair potentials. The spin part will be taken into account later on. The pair potentials in momentum space are illustrated in Fig. 1(b). The pair potential $\Delta_{\boldsymbol{k}}^{(d_{x^2-y^2})}$ is realized in high-T_c superconductor junctions in which the a axis of high-T_c compound is set to be parallel to the x direction. When the a axis is oriented by 45° from the x direction, the pair potential is described by $\Delta_{\boldsymbol{k}}^{(d_{xy})}$. The p-wave symmetry is a possible candidate in organic superconductors,[36–38] Sr_2RuO_4,[39] and heavy-fermion superconductors.

The constructive interference of a quasiparticle enables the formation of the MARS at junction interfaces when a relation

$$\Delta_{k_x,k_y}\Delta_{-k_x,k_y} < 0 \tag{6}$$

is satisfied.[11,13] The pair potentials in Eqs. (3) and (5) satisfy Eq. (6) for all wave numbers. Actually, the low-temperature anomaly of the Josephson current has been reported[15–18,24,25] in SIS junctions of these symmetries.

The absence of the proximity effect in diffusive normal metals is described by a relation[26–28]

$$\Delta_{k_x,k_y} = -\Delta_{k_x,-k_y}. \tag{7}$$

The pair potentials in Eqs. (3) and (4) satisfy Eq. (7). In Fig. 1(b), we classify the pairing symmetries into four groups by the presence (○) or absence (×) of the two interference effects.[30,31] We note that s- and $d_{x^2-y^2}$-wave symmetries belong to the same group.

III. MODEL

Let us consider superconductor/normal-metal/superconductor junctions of the two-dimensional tight-binding model as shown in Fig. 1(a). A vector $\boldsymbol{r} = j\boldsymbol{x} + m\boldsymbol{y}$ points to a lattice site, where $\boldsymbol{x}$ and $\boldsymbol{y}$ are unit vectors in the x and y directions, respectively. The junction consists of three regions: a normal metal (i.e., $1 \le j \le L_N$) and two superconductors (i.e., $-\infty \le j \le 0$ and $L_N+1 \le j \le \infty$). In the y direction, we assume the periodic boundary condition. The number of lattice sites in the y direction is W. Electronic states in superconducting junctions are described by the mean-field Hamiltonian

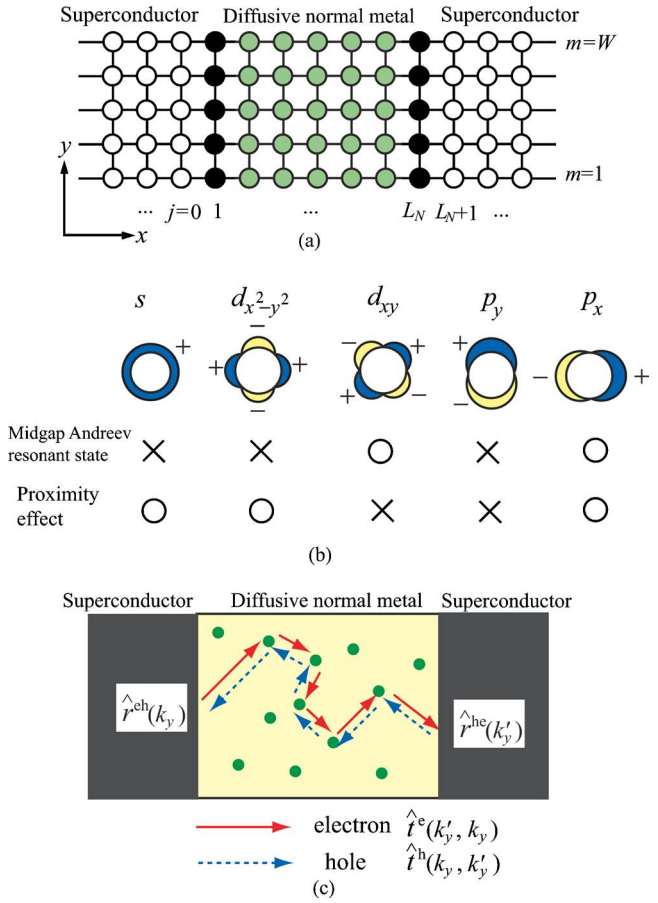

FIG. 1. (Color online) A schematic figure of SNS junctions of the tight-binding model is shown in (a). We illustrate the pair potentials in momentum space in (b). In (c), a propagation process in a diffusive normal metal is illustrated, where solid circles represent impurities.

$$H_{\mathrm{BCS}} = \frac{1}{2}\sum_{\boldsymbol{r},\boldsymbol{r}'}[\tilde{c}_{\boldsymbol{r}}^{\dagger}h_{\boldsymbol{r},\boldsymbol{r}'}\tilde{c}_{\boldsymbol{r}'} - \tilde{c}_{\boldsymbol{r}}^{t}h_{\boldsymbol{r},\boldsymbol{r}'}^{*}\{\tilde{c}_{\boldsymbol{r}'}^{\dagger}\}^{t}] + \frac{1}{2}\sum_{\boldsymbol{r},\boldsymbol{r}'\in \mathrm{S}}[\tilde{c}_{\boldsymbol{r}}^{\dagger}\hat{\Delta}_{\boldsymbol{r},\boldsymbol{r}'}\{\tilde{c}_{\boldsymbol{r}'}^{\dagger}\}^{t} - \{\tilde{c}_{\boldsymbol{r}}\}^{t}\hat{\Delta}_{\boldsymbol{r},\boldsymbol{r}'}^{*}\tilde{c}_{\boldsymbol{r}'}], \tag{8}$$

$$h_{\boldsymbol{r},\boldsymbol{r}'} = -t\delta_{|\boldsymbol{r}-\boldsymbol{r}'|=1} + (\epsilon_{\boldsymbol{r}} - \mu + 4t)\delta_{\boldsymbol{r},\boldsymbol{r}'}, \tag{9}$$

$$\hat{\Delta}_{\boldsymbol{r},\boldsymbol{r}'} = e^{i\varphi_j} \times \begin{cases} i\boldsymbol{d}_{\boldsymbol{r},\boldsymbol{r}'}\cdot\hat{\boldsymbol{\sigma}}\hat{\sigma}_2: & \text{triplet}, \\ id_{\boldsymbol{r},\boldsymbol{r}'}\hat{\sigma}_2: & \text{singlet}, \end{cases} \tag{10}$$

$$\tilde{c}_{\boldsymbol{r}} = \begin{pmatrix} c_{\boldsymbol{r},\uparrow} \\ c_{\boldsymbol{r},\downarrow} \end{pmatrix}, \tag{11}$$

where $c^{\dagger}_{\boldsymbol{r},\sigma}$ ($c_{\boldsymbol{r},\sigma}$) is the creation (annihilation) operator of an electron at $\boldsymbol{r}$ with spin $\sigma=$ ($\uparrow$ or $\downarrow$), "S" in the summation means superconductors, and $\hat{\sigma}_j$ with $j=1-3$ are the Pauli matrices. In superconductors, $\epsilon_{\boldsymbol{r}}$ is taken to be zero. Macroscopic phases are given by $\varphi_j=\varphi_L$ in the left superconductor and by $\varphi_j=\varphi_R$ in the right one. The hopping integral t is considered among the nearest-neighbor sites. We assume that t and the Fermi energy μ are common in superconductors and normal metals. In normal metals, the on-site potential is given randomly in the range of $-V_I/2 \le \epsilon_{\boldsymbol{r}} \le V_I/2$. We also introduce the insulating barrier at $j=1$ and $j=L_N$, where $\epsilon_{\boldsymbol{r}}$ is given by V_B. The pair potentials corresponding to Eqs. (1)–(5) are defined in real space,

$$d^{(s)}_{\boldsymbol{r},\boldsymbol{r}'} = \Delta \delta_{j,j'} \delta_{m,m'}, \tag{12}$$

$$d^{(d_{x^2-y^2})}_{\boldsymbol{r},\boldsymbol{r}'} = \frac{\Delta}{2}(\delta_{|j-j'|,1}\delta_{m,m'} - \delta_{j,j'}\delta_{|m-m'|,1}), \tag{13}$$

$$d^{(d_{xy})}_{\boldsymbol{r},\boldsymbol{r}'} = \frac{\Delta}{2}\,\mathrm{sgn}(j-j')\,\mathrm{sgn}(m-m')\,\delta_{|\boldsymbol{r}-\boldsymbol{r}'|,\sqrt{2}}, \tag{14}$$

$$\boldsymbol{d}^{(p_y)}_{\boldsymbol{r},\boldsymbol{r}'} = \frac{\Delta}{2}\,\mathrm{sgn}(m-m')\,\delta_{|m-m'|,1}\delta_{j,j'}\boldsymbol{e}, \tag{15}$$

$$\boldsymbol{d}^{(p_x)}_{\boldsymbol{r},\boldsymbol{r}'} = \frac{\Delta}{2}\,\mathrm{sgn}(j-j')\,\delta_{|j-j'|,1}\delta_{m,m'}\boldsymbol{e}, \tag{16}$$

where $\boldsymbol{e}$ is a unit vector in the spin space. The amplitude of the pair potential at a finite temperature is denoted by Δ. We describe the dependence of Δ on temperatures by the BCS theory. When we calculate the Josephson current, a macroscopic phase factor $e^{i\varphi_L}$ ($e^{i\varphi_R}$) must be multiplied by Eqs. (12)–(16) for a superconductor on the left- (right-) hand side. In numerical simulations, we choose $\boldsymbol{e}=\boldsymbol{e}_3$ in the p-wave symmetries because the following argument is independent of the spin directions of a Cooper pair.

The Hamiltonian is diagonalized by the Bogoliubov transformation

$$\begin{bmatrix} \tilde{c}_{\boldsymbol{r}} \\ \{\tilde{c}^{\dagger}_{\boldsymbol{r}}\}^t \end{bmatrix} = \sum_{\lambda} \begin{bmatrix} \hat{u}_{\lambda}(\boldsymbol{r}) & \hat{v}^*_{\lambda}(\boldsymbol{r}) \\ \hat{v}_{\lambda}(\boldsymbol{r}) & \hat{u}^*_{\lambda}(\boldsymbol{r}) \end{bmatrix} \begin{bmatrix} \tilde{\gamma}_{\lambda} \\ \{\tilde{\gamma}^{\dagger}_{\lambda}\}^t \end{bmatrix}, \tag{17}$$

$$\tilde{\gamma}_{\lambda} = \begin{pmatrix} \gamma_{\lambda,\uparrow} \\ \gamma_{\lambda,\downarrow} \end{pmatrix}, \tag{18}$$

where $\gamma^{\dagger}_{\lambda,\sigma}$ ($\gamma_{\lambda,\sigma}$) is the creation (annihilation) operator of a Bogoliubov quasiparticle. The wave functions, $\hat{u}_{\lambda}$ and $\hat{v}_{\lambda}$, satisfy the Bogoliubov–de Gennes (BdG) equation[40]

$$\sum_{\boldsymbol{r}'} \begin{bmatrix} h_{\boldsymbol{r},\boldsymbol{r}'}\hat{\sigma}_0 & \hat{\Delta}_{\boldsymbol{r},\boldsymbol{r}'} \\ -\hat{\Delta}^*_{\boldsymbol{r},\boldsymbol{r}'} & -h^*_{\boldsymbol{r},\boldsymbol{r}'}\hat{\sigma}_0 \end{bmatrix} \begin{bmatrix} \hat{u}_{\lambda}(\boldsymbol{r}') \\ \hat{v}_{\lambda}(\boldsymbol{r}') \end{bmatrix} = E_{\lambda} \begin{bmatrix} \hat{u}_{\lambda}(\boldsymbol{r}) \\ \hat{v}_{\lambda}(\boldsymbol{r}) \end{bmatrix}. \tag{19}$$

The eigenvalue E_{λ} is independent of spin channels because we consider unitary states in superconductors. Here we briefly explain the method to calculate the Josephson current for the $d_{x^2-y^2}$-wave symmetry. The application to other symmetries is straightforward. The BdG equation in Eq. (19) for the $d_{x^2-y^2}$-wave symmetry is decoupled into two equations

$$\sum_{\boldsymbol{r}'} \begin{bmatrix} h_{\boldsymbol{r},\boldsymbol{r}'} & d^{(d_{x^2-y^2})}_{\boldsymbol{r},\boldsymbol{r}'} \\ (d^{(d_{x^2-y^2})}_{\boldsymbol{r},\boldsymbol{r}'})^* & -h^*_{\boldsymbol{r},\boldsymbol{r}'} \end{bmatrix} \begin{bmatrix} (u_{11})_{\lambda}(\boldsymbol{r}') \\ (v_{21})_{\lambda}(\boldsymbol{r}') \end{bmatrix} = E_{\lambda} \begin{bmatrix} (u_{11})_{\lambda}(\boldsymbol{r}) \\ (v_{21})_{\lambda}(\boldsymbol{r}) \end{bmatrix}, \tag{20}$$

where u_{ij} (v_{ij}) represent elements of $\hat{u}$ ($\hat{v}$) in Eq. (17). We omit 11 from u_{11} and 21 from v_{21} because $[u_{21}, v_{11}]^t$ obeys essentially the same equation as Eq. (20). The wave function at the jth lattice sites in the x direction can be represented in a column with $2W$ elements:

$$\boldsymbol{\Psi}_{\lambda}(j) = \begin{pmatrix} u_{\lambda}(j\boldsymbol{x}+1\boldsymbol{y}) \\ \vdots \\ u_{\lambda}(j\boldsymbol{x}+W\boldsymbol{y}) \\ v_{\lambda}(j\boldsymbol{x}+1\boldsymbol{y}) \\ \vdots \\ v_{\lambda}(j\boldsymbol{x}+W\boldsymbol{y}) \end{pmatrix}. \tag{21}$$

For instance, for $j<-2$, the wave function obeys the BdG equation

$$\begin{aligned} &\begin{pmatrix} -t\bar{1} & \frac{\Delta}{2}e^{i\varphi_L}\bar{1} \\ \frac{\Delta}{2}e^{-i\varphi_L}\bar{1} & t\bar{1} \end{pmatrix} \boldsymbol{\Psi}_{\lambda}(j+1) \\ &+ \begin{pmatrix} -E_{\lambda}\bar{1} + \bar{E}_S & \bar{T}_S \\ \bar{T}^{\dagger}_S & -E_{\lambda}\bar{1} - \bar{E}_S \end{pmatrix} \boldsymbol{\Psi}_{\lambda}(j) \\ &+ \begin{pmatrix} -t\bar{1} & \frac{\Delta}{2}e^{i\varphi_L}\bar{1} \\ \frac{\Delta}{2}e^{-i\varphi_L}\bar{1} & t\bar{1} \end{pmatrix} \boldsymbol{\Psi}_{\lambda}(j-1) = 0, \end{aligned} \tag{22}$$

$$\bar{T}_S = -\frac{\Delta}{2}e^{i\varphi_L}\bar{h}_0, \tag{23}$$

$$\bar{E}_S = (-\mu + 4t)\bar{1} - t\bar{h}_0, \tag{24}$$

$$\bar{h}_0 = \begin{pmatrix} 0 & 1 & 0 & \cdots & 1 \\ 1 & 0 & 1 & \cdots & 0 \\ \vdots & \ddots & \ddots & \ddots & \vdots \\ 0 & \cdots & 1 & 0 & 1 \\ 1 & 0 & \cdots & 1 & 0 \end{pmatrix}, \tag{25}$$

where $\overline{\cdots}$ denotes $W \times W$ matrices and $\bar{1}$ is the unit matrix. To solve the BdG equation, we apply the recursive Green function method[32–34] and calculate the Matsubara Green function in a $2W \times 2W$ matrix form

$$\check{G}_{\omega_n}(j,j') = \sum_{\lambda} \mathbf{\Psi}_{\lambda}(j)[i\omega_n - E_{\lambda}]^{-1}\mathbf{\Psi}_{\lambda}^{\dagger}(j'). \tag{26}$$

The Josephson current in the normal metal $(1 < j < L_N - 1)$ is given by[32,33]

$$J(j) = -ietT\sum_{\omega_n} \mathrm{Tr}[\check{G}_{\omega_n}(j+1,j) - \check{G}_{\omega_n}(j,j+1)]. \tag{27}$$

We note that $J(j)$ is independent of j when we consider the direct-current Josephson effect.

In simulations, we first compute the Josephson current for a single sample with a specific random potential configuration. After calculating the Josephson current over a number of samples with different random configurations, the ensemble average of the Josephson current and its fluctuations are obtained as

$$\langle J \rangle = \frac{1}{N_s}\sum_{i=1}^{N_s} J_i, \tag{28}$$

$$\delta J = \sqrt{\langle J^2 \rangle - \langle J \rangle^2}, \tag{29}$$

where J_i is the Josephson current in the ith sample and N_s is a number of samples. Strictly speaking, N_s should be taken to be infinity. In this paper, we increase N_s until a sufficient convergence of $\langle J \rangle$ and δJ is obtained.

IV. RESULTS

A. Ballistic junctions

Before discussing the Josephson effect through diffusive normal metals, the Josephson current through ballistic metals should be briefly clarified. Throughout this paper, we fix the parameters as $L_N=70$, $W=25$, and $\mu=2.0t$. In Fig. 2, we show current-phase relation (CPR) for the s-, d_{xy}-, p_y-, and p_x-wave symmetries, where $\Delta_0=0.01t$, $T=0.001T_c$, and $\varphi = \varphi_L - \varphi_R$. Impurity potentials are not considered in normal metals (i.e., $V_I=0$), and Josephson currents are calculated for several choices of potential barriers (V_B). In the absence of potential barriers for $V_B=0$, the CPR becomes $J \propto \varphi$ (Refs. 41 and 42) for all pairing symmetries. The ballistic junctions are rather close to the *long limit* because the coherence length (ξ_0) estimated about at 50 lattice constant is slightly smaller than L_N.[41,42] This CPR is a direct consequence of the multiple Andreev reflection[43] in low temperatures. In general, Josephson currents can be decomposed into a series of

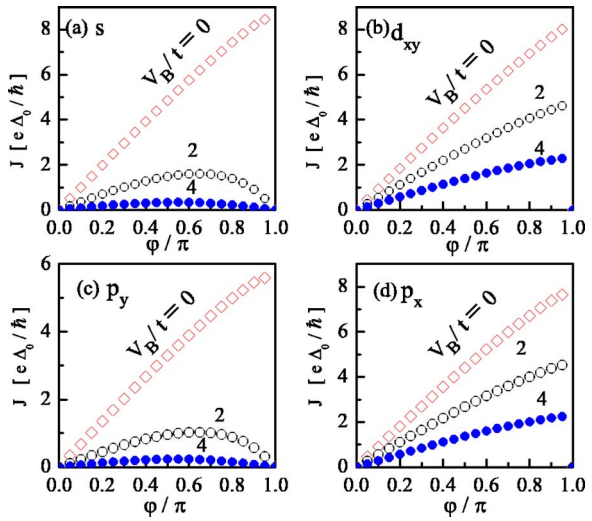

FIG. 2. (Color online) Current-phase relations in ballistic SNS junctions are shown for several choices of potential barriers (V_B), where $T/T_c=0.001$ and $\Delta_0/t=0.01$. Impurity potentials are fixed at $V_I=0$.

$$J = \sum_{n=1}^{\infty} J_n \sin(n\varphi). \tag{30}$$

The components of J_n for $n \geq 2$ represent contributions of the multiple Andreev reflection. Roughly speaking, J_n is proportional to $\{T_N\}^n$, where T_N is the transmission probability of a quasiparticle from the left superconductor to the right superconductor through the normal segment (including two barriers and a normal metal).[44] Thus the multiple Andreev reflection is negligible (i.e., $J_1 \gg J_2 \gg J_3 \gg \cdots$) for $T_N \ll 1$. On the other hand, in the case of $T_N=1$, the multiple Andreev reflection leads to the deviation of current-phase relations from the sinusoidal function. It is noted at $T_N=1$ that we obtain $J \propto \varphi$ and $J \propto \sin(\varphi/2)$ at zero temperature for $L_N \gg \xi_0$ and $L_N \ll \xi_0$, respectively[41,42,45] (see also Appendix B). The results of the CPR are close to the sinusoidal function as the increase of V_B in the s- and p_y-wave junctions because T_N is suppressed by the potential barriers at $j=1$ and L_N and contributions of the multiple Andreev reflection become small in the limit of large V_B. On the other hand, in the d_{xy}- and p_x-wave symmetries, CPR's remain unchanged from $J \propto \varphi$ even in the presence of potential barriers. The multiple Andreev reflection is not suppressed in these symmetries because a transmission probability of insulating barriers is kept to unity due to the resonant tunneling through the MARS's.

In ballistic SNS junctions, the characteristic behavior of Josephson currents depends on the presence or absence of the MARS as shown in Fig. 1(b). We have confirmed that calculated results of the CPR in the $d_{x^2-y^2}$-symmetry show qualitatively the same behavior as those in the s- and p_y-wave symmetries.

B. Diffusive junctions

In Fig. 3, we show the CPR in disordered junctions at $V_B=2t$, where $\Delta_0=0.01t$ and $T=0.001T_c$. At $V_I=2t$, normal

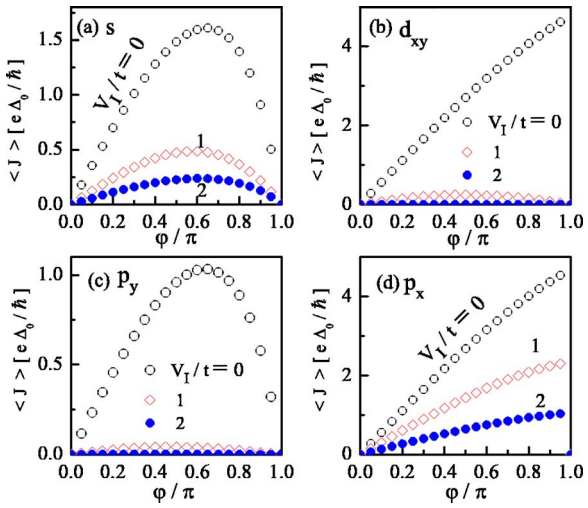

FIG. 3. (Color online) Current-phase relations in disordered SNS junctions are shown for several choices of impurity potentials (V_I), where $T/T_c=0.001$ and $\Delta_0/t=0.01$. The barrier potential is fixed at $V_B=2t$. At $V_I=2t$, normal metals are in the diffusive transport regime.

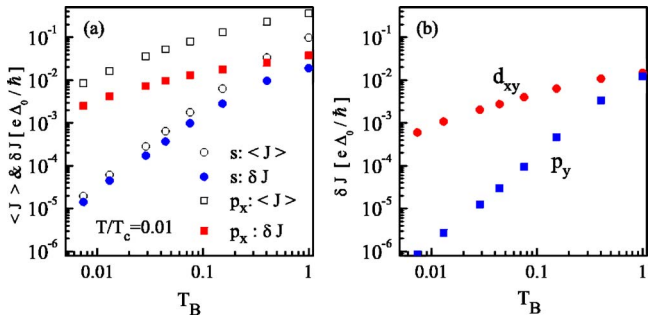

FIG. 4. (Color online) Ensemble average of Josephson current $\langle J\rangle$ and their fluctuations δJ are plotted as a function of transmission probability of potential barrier in the normal state T_B. Results for the s- and p_x-wave symmetries are shown in (a). In (b), only δJ for the d_{xy}- and p_y-wave symmetries are shown because $\langle J\rangle$ is much smaller than δJ. Note that the scales of (a) and (b) are identical to each other.

metals are in the diffusive transport regime. The mean free path is about $\ell\sim 6$ lattice constants and the Thouless energy E_{Th} is calculated to be $1.6\times 10^{-3}t$. The amplitudes of Josephson currents decrease with the increase of V_I in the s-wave junctions as shown in (a). Impurity potentials decrease the transmission probability of normal metals and therefore the amplitude of Josephson current. The ensemble average of Josephson currents for the d_{xy}-wave symmetry rapidly decreases with the increase of V_I and vanishes in the diffusive limit. The same tendency can be seen in the p_y-wave symmetry. In the d_{xy}- and p_y-wave symmetries, no Cooper pair exists in normal metals because the proximity effect is absent there.

In diffusive SNS junctions, it is reasonable to consider that the proximity effect governs the characteristic behavior of Josephson current. In the d_{xy}- and p_y-wave symmetries, a relation $\langle J\rangle\sim 0$ is a natural consequence of the no proximity effect in diffusive metals. Thus it may be also reasonable to expect that the CPR in the p_x-wave symmetry would be close to the sinusoidal function in the presence of impurity potentials. The calculated results in (d), however, show that the CPR almost remains unchanged from $J\propto\varphi$ even in the diffusive limit. This implies that a quasiparticle is not scattered by impurity potentials at all. In the next subsection, we discuss the anomalous properties of Josephson current in the p_x-wave symmetry much further. Different from the s-wave symmetry, the MARS exists in the p_x-wave junctions as discussed in Fig. 1(b). The role of the MARS in the anomalous Josephson effect is explained in Sec. V.

Before turning to the anomalous Josephson effect in the p_x-wave symmetry, the fluctuations of Josephson current are clarified. In Fig. 4(a), we show the maximum amplitude of $\langle J\rangle$ and δJ for the s- and p_x-wave symmetries are plotted, where T_B is the transmission probability of potential barrier at interface in the normal state. Here we choose several values of the barrier potentials V_B at $j=1$ and L_N. For instance, the resulting normal transmission probabilities of the barrier T_B are 1.0, 0.075, and 0.013 for $V_B/t=0$, 6, and 15, respectively. In the s-wave symmetry at $T_B=1$, δJ is close to analytical results of fluctuations.[46,47] The amplitudes of fluctuations decrease with decreasing T_B for both the s- and p_x-wave junctions. For $T_B\ll 1$, $\langle J\rangle$ is close to δJ in the s-wave symmetry, whereas $\langle J\rangle$ is sufficiently larger than δJ in the p_x-wave symmetry. In (b), we show δJ for the d_{xy}- and p_y-wave symmetries at $\varphi=\pi/2$. Since the proximity effect is absent, we find a relation $|\langle J\rangle|\ll\delta J$.[48] This relation does not mean the absence of Josephson current in a single sample measured in experiments.[27] After calculating the Josephson current over a number of different samples, we find that about 50% of them are 0 junctions and the rest of them become π junctions. As a consequence $|\langle J\rangle|$ becomes much smaller than δJ. Thus Josephson current flows in a single sample although the direction of current depends on microscopic configurations of impurities. In Fig. 4(b), δJ represents the typical amplitude of Josephson current in a single sample. When we compare δJ in the d_{xy}-wave symmetry in (b) and $\langle J\rangle$ in the s-wave symmetry in (a), the amplitude of Josephson current in a single d_{xy}-wave junction is expected to be much larger than that in an s-wave junction in the limit of $T_B\ll 1$. This is because the MARS is forming at junction interfaces.[26] In diffusive SNS junctions, the Josephson effect in the d_{xy}-wave symmetry is distinguished from that in the p_y-wave symmetry by the amplitude of fluctuations.

C. Anomalous Josephson effect in p_x-wave symmetry

At first we show that the maximum amplitudes of Josephson currents in the p_x-wave symmetry $J_c(p_x)$ become much larger than those in the s-wave symmetry $J_c(s)$. In Fig. 5(a), the ratios $J_c(p_x)/J_c(s)$ at $\Delta_0=0.1t$ are plotted as a function of temperature for several choices of T_B. The ratios $J_c(p_x)/J_c(s)$ increase with decreasing T and amazingly become more than 100 in low temperatures for small T_B. The amplitudes of Josephson currents in the p_x-wave junctions are much larger than those in the s-wave junctions. In Fig. 5(b), J_cR_N normalized by $\pi\Delta_0/e$ is plotted as a function of T_B at $T=0.001T_c$,

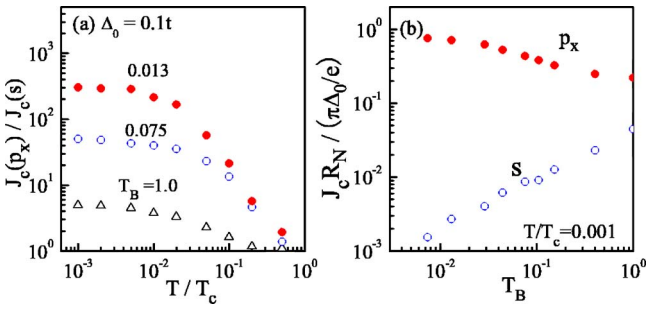

FIG. 5. (Color online) The maximum amplitudes of Josephson currents in the p_x-wave symmetry $J_c(p_x)$ are compared with those in the s-wave symmetry $J_c(s)$ in (a), where T_B is the transmission probability of potential barriers in the normal states. In (b), $J_c(p_x)$ and $J_c(s)$ are plotted as a function of T_B at $T=0.001T_c$.

where R_N is the normal resistance of junctions. The results show that J_cR_N in the s-wave symmetry decreases with decreasing T_B, whereas that in the p_x-wave symmetry increases. It is known that large values of J_c are desired in device applications because J_cR_N limits the operation speeds of Josephson devices. Thus Fig. 5(b) implies high potentials of p-wave junctions as coherent devices.

We next focus on the current-phase relations of the Josephson effect. In Fig. 6, Josephson currents are plotted as a function of φ for the p_x-wave symmetries at $V_B=0$. Parameters are chosen as $\Delta_0=0.01t$ and $0.0001t$ in (a) and (b), respectively. The CPR's are almost a sinusoidal function at a high temperature of $T=0.5T_c$. At $T=0.001T_c$, however, the current-phase relations are close to $J\propto\varphi$ and $J\propto\sin(\varphi/2)$ in (a) and (b), respectively. These are characteristic current-phase relations in ballistic Josephson junctions in the s-wave symmetry.[41,42,45] The results imply large contributions of the multiple Andreev reflection in low temperatures.

In Fig. 6, we also show the current-phase relations in the s-wave symmetry at $T=0.001T_c$ with a solid line. The current-phase relation in the s-wave symmetry is described almost by the sinusoidal function[4,49] because impurity potentials in normal metals suppress T_N (transmission probability of the normal segment in a superconducting state) and therefore multiple Andreev reflections. In the p_x-wave junctions,

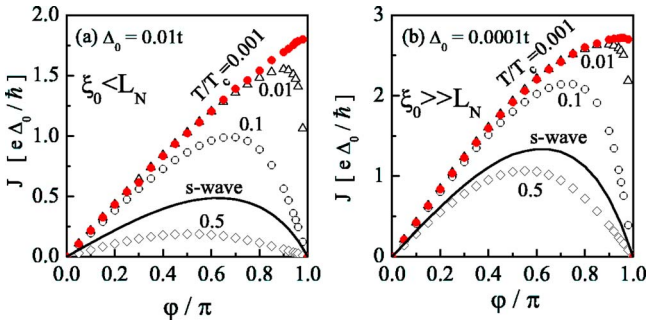

FIG. 6. (Color online) Current-phase relations for the p_x-wave symmetry are shown for several temperatures at $V_B=0$, where $\Delta_0=0.01t$ in (a) and $\Delta_0=0.0001t$ in (b). For comparison, results in the s-wave junctions at $T=0.001T_c$ are shown with a solid line in (a) and (b). The amplitude in the s-wave symmetry is multiplied by 5 in (a).

the coherence length ξ_0 is estimated to be about 50 lattice constants in (a) and 5000 in (b). Thus $L_N > \xi_0$ and $L_N \ll \xi_0$ are satisfied in (a) and (b), respectively. The current-phase relations such as $J\propto\sin(\varphi/2)$ in (b) and $J\propto\varphi$ in (a) are universal properties of the p_x-wave junctions at low temperatures because they are independent of the strength of the barrier potentials and the degree of disorder in normal metals. The calculated results in Fig. 6 indicate $T_N=1$ even in the presence of impurity potentials. The large amplitudes of the Josephson current in Fig. 5 are also explained by $T_N=1$.

V. MARS IN NORMAL METALS

A. Quasiparticle density of states

The calculated results in Figs. 3(d), 5, and 6 show the specific properties of Josephson currents in the p_x-wave junctions. In what follows, we analyze quasiparticle states in normal metals to understand the origin of the anomalous Josephson effect. In Fig. 7, we show the local density of states in normal metals for the s- and p_x-wave symmetries, where $\Delta_0=0.005t$, $\gamma=0.05\Delta_0$, and N_0 denotes the normal density of states. The local density of states is calculated from

$$N(E,j) = -\,\mathrm{Im}\,\mathrm{Tr}\,\check{G}_{E+i\gamma}(j,j)/\pi, \tag{31}$$

where E is measured from the Fermi energy and γ is a small imaginary part. At $\varphi=0$ in the s-wave junctions in (a), the local density of states for $E<E_{Th}\sim 0.3\Delta_0$ is suppressed because of the proximity effect. The suppression of the local density of states indicates the conversion of quasiparticles to Cooper pairs in normal metals. At $\varphi=\pi$ in (b), the local density of states recovers its amplitude for $E<E_{Th}$. The wave functions of Cooper pairs from the left superconductor and from the right one cancel each other around $\varphi\sim\pi$ as schematically illustrated in Fig. 8.

The local density of states is drastically changed in the p_x-wave symmetry as shown in Fig. 8(c) and 8(d). Zero-energy peaks whose width is determined by γ can be seen, which means the formation of the midgap Andreev resonant state in normal metals. Although the MARS originally localizes at junction interfaces,[11] the MARS penetrates into normal metals in the presence of the proximity effect. Spatial profiles of the local density of states depend remarkably on the external phase difference as shown in Figs. 8(c) and 8(d). At $\varphi=0$, the zero-energy peak disappears at the center of normal metals ($j\sim 35$) because the wave functions of the MARS from the left superconductors cancel out that from the right one as shown schematically in a lower panel in Fig. 8(c). On the other hand, in Fig. 8(d), the wave functions of the MARS in the two superconductors have the same sign with each other. Thus the two MARS's can penetrate deeply into normal metals and the zero-energy peak can be seen everywhere. We note that the penetration of the MARS is possible only when the proximity effect is present in normal metals. In fact, we have confirmed that no zero-energy peak is found in normal metals in the d_{xy}-wave symmetry as shown in Fig. 8(a), where the LDOS for d_{xy}-wave and p_y-wave symmetries are plotted for $j=0-71$ in Figs. 8(a) and 8(b), respectively. In normal metals for $j=1\sim 70$, the LDOS

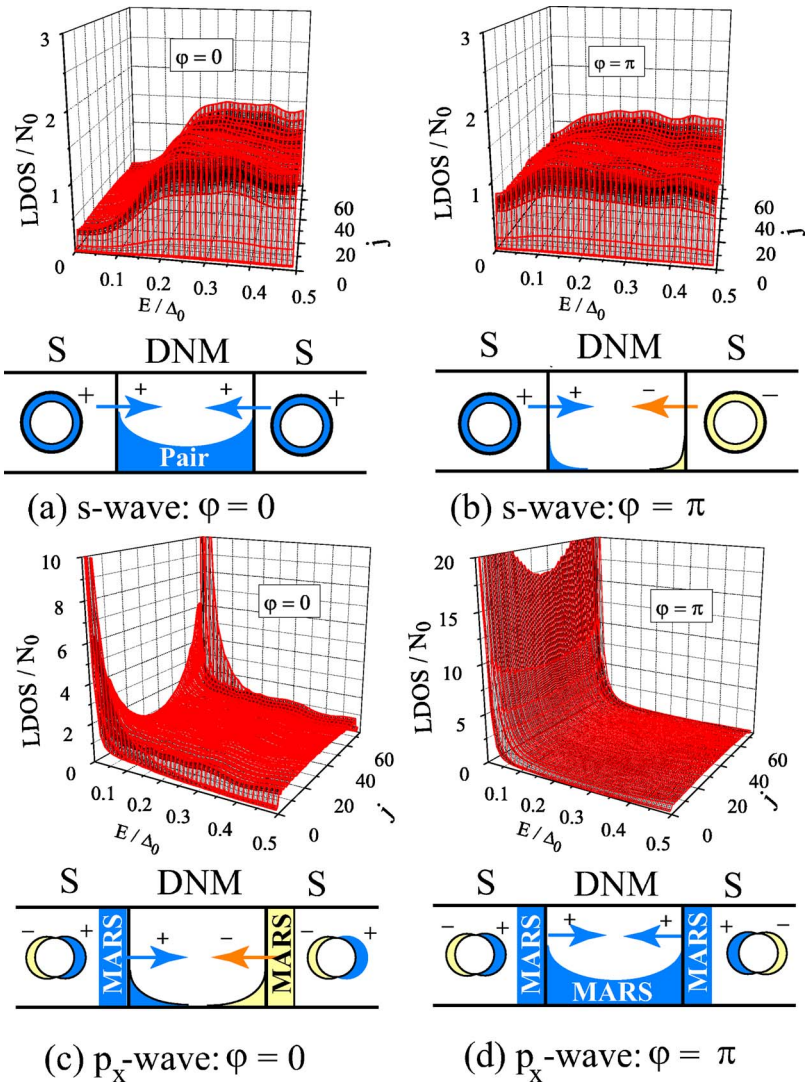

FIG. 7. (Color online) Local density of states (LDOS) in normal metals ($0 \leq j \leq L_N = 71$) is shown for the s-wave and p_x-wave symmetries. The left and right superconductors are attached at $j=0$ and $j=71$, respectively. Note that E_{Th} is about $0.3\Delta_0$. In schematic pictures, DNM and S denote a diffusive normal metal and a superconductor, respectively. The local density of states shown here is calculated in the absence of Josephson currents. We have confirmed that the results at $\varphi = 0.99\pi$ qualitatively show the same behavior as those at $\varphi = \pi$.

becomes almost a flat structure around $E \sim 0$ in both d_{xy}- and p_y-wave symmetries because the proximity effect is absent there. In the d_{xy}-wave symmetry, zero-energy peaks in LDOS at $j=0$ and 71 indicate the formation of the MARS in superconductors and are responsible for the large fluctuations shown in Fig. 4(b). Figure 7 indicates that the proximity effects bridges the two MARS's in the two superconductors.

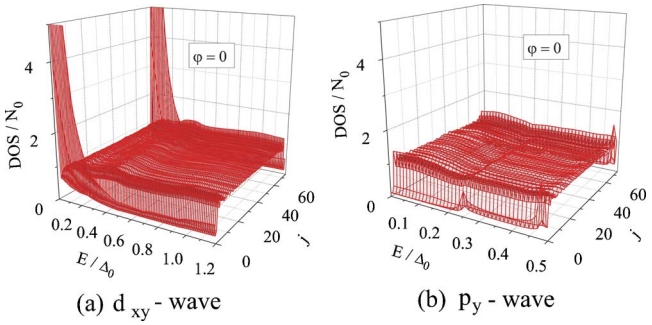

FIG. 8. (Color online) Local density of states at $\varphi=0$ in normal metals are shown for the d_{xy}-wave and p_y-wave symmetries in (a) and (b), respectively. In the d_{xy} symmetry, zero-energy peaks at $j=0$ and 71 correspond to the MARS.

Thus $T_N=1$ holds because of the resonant transmission through the MARS in normal metals. The Josephson effect specific to the p_x-wave symmetry discussed in Figs. 5 and 6 are a consequence of the diffusion of the MARS *into* normal metals.[50]

B. Cooper pairs in diffusive normal metals

In normal metals, pair potentials are always zero because of no pairing interaction. The proximity effect means finite Cooper pair amplitudes in normal metals. When the Green function in Eq. (26) is expressed by

$$\check{G}_{\omega_n}(j,j') = \begin{pmatrix} \bar{a}_{\omega_n}(j,j') & \bar{b}_{\omega_n}(j,j') \\ \bar{c}_{\omega_n}(j,j') & \bar{d}_{\omega_n}(j,j') \end{pmatrix}, \tag{32}$$

pair amplitudes at j are calculated to be $\mathrm{Tr}\,\bar{b}_{\omega_n}(j,j)$. In superconductors, the pair amplitude is an even function of ω_n irrespective of pairing symmetries. In the s-wave symmetry, the pair amplitude in a diffusive normal metal is also an even function of ω_n. In the p_x-wave symmetry, however, we confirmed that the pair amplitude becomes an odd function of ω_n

in a diffusive normal metal. Thus odd-frequency pairs carry the anomalous Josephson current. This is a consequence of Pauli's principle in quantum mechanics. A general theory of the odd-frequency pairs in proximity structures will be given elsewhere.[51]

VI. CONCLUSION

We have numerically studied the Josephson current in superconductor/diffusive-normal-metal/superconductor junctions by using the recursive Green function method. In superconductors, we assume s-, d_{xy}-, p_y-, and p_x-wave pairing symmetries. These pair potentials are classified into different groups by the presence or absence of two interference effects: a midgap Andreev resonant state at junction interfaces and the proximity effect in diffusive normal metals as shown in Fig. 1(b). In the d_{xy}- and p_y-wave symmetries, the ensemble average of the Josephson current vanishes (i.e., $|\langle J\rangle| \ll \delta J$) for all temperatures because the proximity effect is absent in diffusive normal metals.

The Josephson current in the p_x-wave symmetry is much larger than that in the s-wave in low temperatures. In the p_x-wave symmetry, current-phase relations in low temperatures are close to those in ballistic junctions such as $J \propto \sin(\varphi/2)$ and $J \propto \varphi$ independent of the strength of potential barriers at interfaces and the degree of disorder in normal metals. This is a consequence of a cooperative effect between the MARS at junction interfaces and the proximity effect in diffusive normal metals. The two midgap Andreev resonant states penetrate deeply into normal metals and causes the unusual Josephson effect in the p_x-wave superconducting junctions. The anomalous Josephson effect is a novel feature of phase-sensitive transport in spin-triplet superconducting junctions.

ACKNOWLEDGMENTS

This work has been partially supported by a Grant-in-Aid for the 21st Century COE program on "Topological Science and Technology" and "Frontiers of Computational Science" and a Grant-in-Aid for Scientific Research on Priority Area "Physics of new quantum phases in superclean materials" (Grant No. 18043001) from The Ministry of Education, Culture, Sports, Science and Technology of Japan.

APPENDIX A: NORMAL CONDUCTANCE

In this appendix, the normal conductance in disordered wires is summarized. We fix two parameters such as $V_I = 2.0t$ and $\mu = 2.0t$. In Fig. 9, we show the conductance of the normal segment at zero temperature as a function of L_N by using the usual recursive Green function method.[34] When the normal metals are in the quasi ballistic regime, $\langle g_N\rangle(L_N)/W$ is proportional to L_N because $\langle g_N\rangle \propto N_c$. Here N_c is the number of propagating channels, which is almost proportional to W. When the normal metals are in the diffusive transport regime, $\langle g_N\rangle(L_N)/W$ becomes $k_F\ell/2$ independent of L_N, where ℓ is the elastic mean free path. When the normal metals are in the localization regime, $\langle g_N\rangle L_N/W$ decreases with increasing L_N like $\exp(-L_N/\xi_L)$, where ξ_L is the localization length. Thus, in Fig. 9, the quasiballistic, the diffusive, and the localization regimes correspond to $L_N < 50$, $60 < L_N < 110$, and $L_N \gg 110$, respectively. In the diffusive regime, all data in (a) should be close to a single curve irrespective of W. The results, however, slightly depend on W because of finite-size effects. Strictly speaking, N_c is not exactly proportional to W. From the numerical results for $W=25$ in the diffusive regime, we estimate the mean free path as $\ell \sim 6$ lattice constants. When we fix L_N at 70, the Thouless energy E_{Th} is estimated to be $1.6 \times 10^{-3}t$.

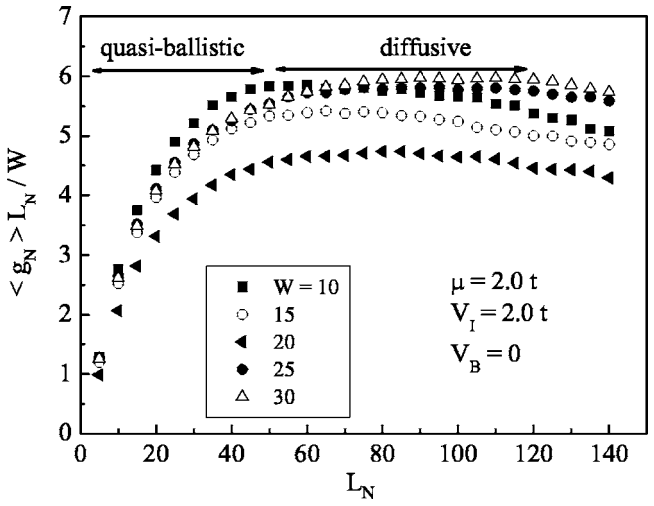

FIG. 9. The normal conductance versus the length of disordered region is plotted, where $V_I = 2.0t$, $\mu = 2.0t$, and $V_B = 0$.

APPENDIX B: CURRENT-PHASE RELATION AT $T=0$

The relation between the pairing symmetries and the proximity effect can be understood by an analytical expression of the Josephson current.[19,26,27] The Josephson current is decomposed into a series as shown in Eq. (30). The components of Josephson current can be represented approximately by a formula[19]

$$J_n \sin(n\varphi) = -2e\,\mathrm{Im} \sum_{k_y}{}' \sum_{k_y}{}' T \sum_{\omega_n} \mathrm{Tr} \times [(\hat{r}^{eh}(k_y) \cdot \hat{t}^{h}_{k_y,k_y'} \cdot \hat{r}^{he}(k_y') \cdot \hat{t}^{e}_{k_y',k_y})^n], \quad \text{(B1)}$$

where $\hat{r}^{eh}(k_y)$ $[\hat{r}^{he}(k_y')]$ is the Andreev reflection coefficient[43] from a hole to an electron at the left interface [from an electron to a hole at the right interface] and $\hat{t}^{e}$ $[\hat{t}^{h}]$ is the transmission coefficient in a diffusive normal metal in the electron [hole] branch. The propagation process is schematically illustrated in Fig. 1(c). At the left (right) interface, k_y (k_y') characterizes a transverse momentum (a transport channel) on the Fermi surface. The summation Σ_{k_y}' runs over wave numbers k_y on the Fermi surface with $k_x > 0$.

When we consider a δ-function potential barrier at the interface, $V(\boldsymbol{r}) = V_0\delta(\boldsymbol{r})$, we obtain expressions of the Andreev reflection coefficients[19]

$$\hat{r}^{eh}(k_y) = -i\bar{k}_x^2 \frac{t_B K}{\Xi} \nu \hat{\Delta}_{\boldsymbol{k}} e^{i\varphi_L}, \tag{B2}$$

$$\hat{r}^{he}(k_y) = -i\left[\frac{t_B K}{\Xi} \nu \hat{\Delta}_{\boldsymbol{k}}\right]^{\dagger} e^{-i\varphi_R}, \tag{B3}$$

$$K = \sqrt{(\omega_n)^2 + \Delta_{\boldsymbol{k}}^2} - |\omega_n|, \tag{B4}$$

$$\Xi = \Delta_{\boldsymbol{k}}^2 \nu + (1 - t_B) K^2, \tag{B5}$$

$$\hat{\Delta}_{\boldsymbol{k}} = \begin{cases} i\Delta_{\boldsymbol{k}} \hat{\sigma}_2: & \text{singlet}, \\ i\Delta_{\boldsymbol{k}} (\boldsymbol{e} \cdot \hat{\boldsymbol{\sigma}}) \hat{\sigma}_2: & \text{triplet}, \end{cases} \tag{B6}$$

where $t_B = \bar{k}_x^2/(z_0^2 + \bar{k}_x^2)$ is the transmission probability of the barrier for a wave number $(\bar{k}_x, \bar{k}_y)$, $z_0 \equiv V_0/\hbar v_F$ represents the strength of the potential barrier, $\hat{\sigma}_j$ with $j=1-3$ are the Pauli matrices, and $\Delta_{\boldsymbol{k}}$ is given in Eqs. (1)–(5). Here we assume that $\Delta_{-k_x,k_y} = \nu \Delta_{k_x,k_y}$ with $\nu = \pm 1$. The pair potentials in Eqs. (1), (2), and (4) belong to $\nu=1$, whereas Eqs. (3) and (5) belong to $\nu=-1$. The spin part of Cooper pairs is taken into account through a matrix representation of the pair potential in Eq. (B6).The transmission coefficients in normal metals are spin diagonal (i.e., $\hat{t}^{e(h)} = t^{e(h)} \hat{\sigma}_0$) in the absence of spin-flip scatterings, where $\hat{\sigma}_0$ is the 2×2 unit matrix. The ensemble average of $t^e_{k_y',k_y} t^h_{k_y,k_y'}$ can be represented by the Cooperon propagator because the propagation paths of a hole are the time-reversal propagation paths of an electron as shown in Fig. 1(c). In diffusive normal metals, the transmission coefficients after the ensemble average are calculated as

$$\langle (t^e_{k_y',k_y} t^h_{k_y,k_y'})^n \rangle \simeq \frac{1}{N_c^2} \langle g_N(nL_N) \rangle \frac{\eta(nL_N)}{\sinh \eta(nL_N)}, \tag{B7}$$

$$\eta(L_N) = \sqrt{\frac{\omega_n}{\pi T}} \frac{L_N}{\xi_D} = \sqrt{\frac{2\omega_n}{E_{Th}}}, \tag{B8}$$

$$\langle g_N(L_N) \rangle = \frac{W}{L_N} \pi N_0 D_0, \tag{B9}$$

where $\langle \cdots \rangle$ denotes the ensemble average, $N_c = (Wk_F/\pi)$ is the number of propagating channels, N_0 is the density of states per unit area, and W is the width of junctions. In diffusive normal metals, $\xi_D = \sqrt{D_0/2\pi T}$ is the coherence length and $\langle G_N \rangle = (2e^2/h)\langle g_N \rangle$ is the ensemble average of the normal conductance. After the ensemble average, the transmission coefficients are independent of k_y and k_y'. We note that $\eta/\sinh \eta$ represents a degree of phase coherence in normal metals. The phase coherence in normal metals is perfect (i.e., $\eta/\sinh \eta = 1$) at zero temperature. The phase coherence is suppressed in high temperatures such as $\omega_n \gg E_{Th}$.

After a small amount of algebra, we find

$$\langle J_1 \rangle = 4eT \sum_{\omega_n} \langle g_N \rangle \frac{\eta}{\sinh \eta} I_1^2, \tag{B10}$$

$$I_n = \frac{1}{N_c} \sum_{k_y}{}' \left\{ \frac{t_B K \nu}{\Xi} \Delta_{\boldsymbol{k}} \right\}^n, \tag{B11}$$

where I_1 corresponds to the Andreev reflection coefficient averaged over all propagating channels. We find $I_1 = 0$ for the d_{xy}- and p_y-wave symmetries because $\bar{k}_x^2 K/\Xi$ is an even function of k_y and $\Delta_{\boldsymbol{k}}$ is an odd function of k_y. Since $\langle J_1 \rangle \propto I_1^2$, the ensemble average of J_1 vanishes, which represents the absence of the proximity effect. Even in unconventional superconductor junctions, Cooper pairs penetrate into normal metals. However, Cooper pairs in normal metals are characterized not only by the amplitude but also by the sign degree of freedom. When Eq. (7) holds, Cooper pairs with positive sign and those with negative sign cancel each other out in diffusive normal metals.

In the presence of the MARS, the expansion in Eq. (B1) has less validity. The effects of the MARS on the Josephson current, however, can be roughly understood with the following argument. In the limit of $\omega_n \to 0$ and $t_B \ll 1$, we find

$$\frac{t_B K \nu \Delta_{\boldsymbol{k}}}{\Xi} \to \begin{cases} \dfrac{t_B}{2} \dfrac{\Delta_{\boldsymbol{k}}}{\sqrt{\omega_n^2 + \Delta_{\boldsymbol{k}}^2}}, & \nu = 1, \\ \dfrac{t_B \Delta_{\boldsymbol{k}}}{2|\omega_n| + t_B |\Delta_{\boldsymbol{k}}|}, & \nu = -1. \end{cases} \tag{B12}$$

For $\nu=-1$, the Andreev reflection coefficient becomes unity independent of t_B in the limit of $\omega_n \to 0$. The Josephson current in the presence of the MARS is expected to be anomalous at low temperatures because of the rapid increase of I_1 with the decrease of $\omega_n \propto T$.

In the case of s-wave symmetry, the characteristic CPR at the zero temperature can be derived from Eq. (B1). In ballistic junctions, transmission coefficients are approximately given by

$$t^h_{k_y,k_y'} t^e_{k_y',k_y} = \delta_{k_y',k_y} \exp(-2\omega_n L_N/v_F). \tag{B13}$$

At $T=0$, $t^h_{k_y,k_y'} t^e_{k_y',k_y}$ corresponds to the transmission probability in the normal segment and becomes unity (i.e., $T_N = 1$). Thus we obtain, at $z_0 = 0$,

$$J_n = 4e(-1)^{n+1} T \sum_{\omega_n} \sum_{k_y}{}' e^{-2\omega_n L_N n/v_F} \times \left(\frac{\sqrt{\omega_n^2 + \Delta_0^2} - |\omega_n|}{\Delta_0} \right)^{2n}. \tag{B14}$$

The summation of ω_n can be replaced by the integration at $T=0$. We obtain

$$J_n = \begin{cases} N_c \dfrac{2(-1)^{n+1}}{n} \dfrac{e v_F}{\pi L_N} & \text{for } \xi_0 \ll L_N, \\ N_c \dfrac{8(-1)^{n+1}}{(2n+1)(2n-1)\pi} e\Delta_0 & \text{for } \xi_0 \gg L_N. \end{cases} \tag{B15}$$

The CPR are calculated as[41,42,45]

$$J = \begin{cases} N_c \dfrac{ev_F}{L_N}\dfrac{\varphi}{\pi} & \text{for } \xi_0 \ll L_N, \\ N_c e\Delta_0 \sin(\varphi/2) & \text{for } \xi_0 \gg L_N. \end{cases} \tag{B16}$$

When normal metals are in the diffusive limit,

$$J_n = 4e(-1)^{n+1} T \sum_{\omega_n} \frac{\langle g_N(L_N)\rangle}{n} e^{-n\sqrt{2\omega_n/E_{Th}}} \times \left(\frac{\sqrt{\omega_n^2 + \Delta_0^2} - |\omega_n|}{\Delta_0} \right)^{2n} \tag{B17}$$

is obtained from Eqs. (B7)–(B9) at $z_0=0$. For $\Delta_0 \ll E_{Th}$, we find

$$J_n = 4e\langle g_N(L_N)\rangle \frac{\Delta_0}{\pi} \frac{2(-1)^{n+1}}{(2n+1)(2n-1)}. \tag{B18}$$

The CPR

$$J = \frac{4}{\pi} e\Delta_0 \langle g_N(L_N)\rangle \cos(\varphi/2) a \tanh[\sin(\varphi/2)] \tag{B19}$$

coincides with the previous results[49] apart from a numerical factor. In the same way, we obtain

$$J = eE_{Th} \frac{4}{\pi} \langle g_N(L_N)\rangle \sum_{n=1}^{\infty} \frac{(-1)^{n+1}}{n^3} \sin(n\varphi) \tag{B20}$$

for $\Delta_0 \gg E_{Th}$. The results, however, do not coincide with those in Ref. 4. Equation (B20) takes its maximum at $\varphi = 0.58\pi$. On the other hand, the results in Ref. 4 show the maximum around $\varphi = 0.62\pi$ consistently with numerical simulations.

*Electronic address: asano@eng.hokudai.ac.jp

[1] B. D. Josephson, Phys. Lett. **1**, 251 (1962).
[2] K. K. Likharev, Rev. Mod. Phys. **51**, 101 (1979).
[3] V. Ambegaokar and A. Baratoff, Phys. Rev. Lett. **10**, 486 (1963).
[4] A. D. Zaikin and G. F. Zharkov, Sov. J. Low Temp. Phys. **7**, 184 (1981).
[5] C. C. Tsuei and J. R. Kirtley, Rev. Mod. Phys. **72**, 969 (2000).
[6] M. Sigrist and T. M. Rice, J. Phys. Soc. Jpn. **61**, 4283 (1992); Rev. Mod. Phys. **67**, 503 (1995).
[7] D. A. Wollman, D. J. Van Harlingen, W. C. Lee, D. M. Ginsberg, and A. J. Leggett, Phys. Rev. Lett. **71**, 2134 (1993).
[8] L. J. Buchholtz and G. Zwicknagl, Phys. Rev. B **23**, 5788 (1981).
[9] J. Hara and K. Nagai, Prog. Theor. Phys. **76**, 1237 (1986).
[10] C. R. Hu, Phys. Rev. Lett. **72**, 1526 (1994).
[11] Y. Tanaka and S. Kashiwaya, Phys. Rev. Lett. **74**, 3451 (1995).
[12] S. Kashiwaya and Y. Tanaka, Rep. Prog. Phys. **63**, 1641 (2001).
[13] Y. Asano, Y. Tanaka, and S. Kashiwaya, Phys. Rev. B **69**, 134501 (2004).
[14] Y. Asano, Y. Tanaka, and S. Kashiwaya, Phys. Rev. B **69**, 214509 (2004).
[15] Y. Tanaka and S. Kashiwaya, Phys. Rev. B **53**, R11957 (1996).
[16] Y. S. Barash, H. Burkhardt, and D. Rainer, Phys. Rev. Lett. **77**, 4070 (1996).
[17] Y. Tanaka and S. Kashiwaya, Phys. Rev. B **56**, 892 (1997).
[18] Y. Tanaka and S. Kashiwaya, Phys. Rev. B **58**, R2948 (1998).
[19] Y. Asano, Phys. Rev. B **64**, 224515 (2001).
[20] Y. S. Barash, A. M. Bobkov, and M. Fogelström, Phys. Rev. B **64**, 214503 (2001).
[21] Y. Asano and K. Katabuchi, J. Phys. Soc. Jpn. **71**, 1974 (2002).
[22] Y. Asano, Y. Tanaka, M. Sigrist, and S. Kashiwaya, Phys. Rev. B **67**, 184505 (2003); **71**, 214501 (2005).
[23] E. Il'ichev, V. Zakosarenko, R. P. J. Ijsselsteijn, V. Schultze, H.-G. Meyer, H. E. Hoenig, H. Hilgenkamp, and J. Mannhart, Phys. Rev. Lett. **81**, 894 (1998); E. Il'ichev, M. Grajcar, R. Hlubina, R. P. J. Ijsselsteijn, H. E. Hoenig, H. -G. Meyer, A. Golubov, M. H. S. Amin, A. M. Zagoskin, A. N. Omelyanchouk, and M. Yu. Kupriyanov, *ibid.* **86**, 5369 (2001).
[24] H.-J. Kwon, K. Senguputa, and V. M. Yakovenko, Eur. Phys. J. B **37**, 349 (2004).
[25] A. A. Golubov, M. Yu. Kupriyanov, and E. Il'ichev, Rev. Mod. Phys. **76**, 411 (2004).
[26] Y. Asano, Phys. Rev. B **64**, 014511 (2001).
[27] Y. Asano, J. Phys. Soc. Jpn. **71**, 905 (2002).
[28] Y. Tanaka, Yu. V. Nazarov, and S. Kashiwaya, Phys. Rev. Lett. **90**, 167003 (2003).
[29] Y. Tanaka, Yu. V. Nazarov, A. A. Golubov, and S. Kashiwaya, Phys. Rev. B **69**, 144519 (2004).
[30] Y. Tanaka and S. Kashiwaya, Phys. Rev. B **70**, 012507 (2004).
[31] Y. Tanaka, S. Kashiwaya, and T. Yokoyama, Phys. Rev. B **71**, 094513 (2005); Y. Tanaka, Y. Asano, A. A. Golubov, and S. Kashiwaya, Phys. Rev. B **72**, 140503(R) (2005).
[32] A. Furusaki, Physica B **203**, 214 (1994).
[33] Y. Asano, Phys. Rev. B **63**, 052512 (2001).
[34] P. A. Lee and D. S. Fisher, Phys. Rev. Lett. **47**, 882 (1981).
[35] Y. Asano, Y. Tanaka, and S. Kashiwaya, Phys. Rev. Lett. **96**, 097007 (2006).
[36] A. A. Abrikosov, J. Low Temp. Phys. **53**, 359 (1983).
[37] Y. Hasegawa and H. Fukuyama, J. Phys. Soc. Jpn. **56**, 877 (1987).
[38] A. G. Lebed, Phys. Rev. B **59**, R721 (1999); A. G. Lebed, K. Machida, and M. Ozaki, Phys. Rev. B **62**, R795 (2000).
[39] Y. Maeno, H. Hashimoto, K. Yoshida, S. NishiZaki, T. Fujita, J. G. Bednorz, and F. Lichtenberg, Nature (London) **372**, 532 (1994).
[40] P. G. de Gennes, *Superconductivity of Metals and Alloys* (Benjamin, New York, 1966).
[41] C. Ishii, Prog. Theor. Phys. **44**, 1525 (1970); C. Ishii, *ibid.* **47**, 1646 (1972).
[42] J. Bardeen and J. L. Johnson, Phys. Rev. B **5**, 72 (1972).
[43] A. F. Andreev, Zh. Eksp. Teor. Fiz. **46**, 1823 (1964) [Sov. Phys. JETP **19**, 1228 (1964)].
[44] We note that T_N is the transmission probability at the Fermi energy in the *superconducting state*. In the *s*-wave junctions, T_N is almost the same as the transmission probability in the *normal*

state which is calculated from the normal conductance of junctions. In addition, T_N is not sensitive to the energy of a quasiparticle around the Fermi level in the *s*-wave symmetry.

[45] I. O. Kulik and A. N. Omel'yanchuk, Fiz. Nizk. Temp. **3**, 945 (1977) [Sov. J. Low Temp. Phys. **3**, 459 (1977)].

[46] B. L. Al'tshuler and B. Z. Spivak, Pis'ma Zh. Eksp. Teor. Fiz. **65**, 609 (1987) [JETP Lett. **65**, 343 (1987)].

[47] Y. Koyama, Y. Takane, and H. Ebisawa, J. Phys. Soc. Jpn. **66**, 430 (1997).

[48] In numerical simulations for the d_{xy}- and p_y-wave symmetries, $\langle J \rangle$ does not become exactly zero. This is because higher harmonics [i.e., $J_n \sin(n\varphi)$ for $n \geq 2$ in Eq. (30)] contribute to $\langle J \rangle$. We confirm that $|\langle J \rangle|$ is smaller than δJ by at least two orders of magnitude in the present simulation.

[49] I. O. Kulik and A. N. Omel'yanchuk, Pis'ma Zh. Eksp. Teor. Fiz. **21**, 219 (1975) [JETP Lett. **21**, 96 (1975)].

[50] The proximity effect is diagrammatically described by the so-called Cooperon propagator which has a singular behavior at $\omega_n = 0$. The MARS is also characterized by the singular behavior of the Andreev reflection coefficients at $\omega_n = 0$. The penetration of the MARS can be interpreted in terms of an interplay between the two singular behaviors in the Cooperon propagator and the Andreev reflection coefficients.

[51] Y. Tanaka and A. A. Golubov, cond-mat/0606231 (unpublished).